Kime-Phase Tomography and Manifold Representation of Longitudinal Processes over a Complex-Time Domain

Kime-Phase Tomography (KPT) and Induced Space-Kime Analytics

Ivo D. Dinov, Yueyang Shen & Bojko Bakalov

March 8, 2026

SOCR · University of Michigan · North Carolina State University
https://SOCR.umich.edu | https://TCIU.predictive.space/

Outline

1. Motivation and Problem Setting
2. Mathematical Foundations
3. Inference and Space-Kime Analytics
4. Applications and Validation (Simulations)

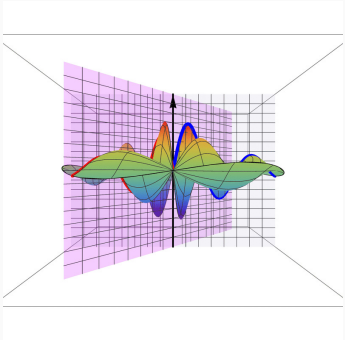

Kime-Surface Representation

1. Motivation and Problem Setting

Why kime? Why tomography?

- **Observed problem:** repeated measurements at the same chronological time often exhibit large *structured* variability (not just additive noise).
- **Consequence:** averaging/denoising can erase latent state structure, leading to miscalibrated inference or degraded prediction.
- **KPT goal:** decompose replicate variability into

  extrinsic (range-space) noise $\quad + \quad$ intrinsic (domain-space) phase variability.

- **Kime representation:** augment time t by a latent phase $\theta \in \mathbb{S}^1$, forming a complex-time coordinate

  $$\kappa \;=\; t\, e^{i\theta} \in \mathbb{C},$$

  enabling *phase-resolved* inference and prediction.

Rationale for Time $\longrightarrow$ Kime Extension

- **Math:** *Time* is a special case of *Kime*, $\kappa = t\, e^{i\theta} \in \mathbb{C}$, where $\theta = 0$. Time ($\mathbb{R}^+$) is a subgroup of the multiplicative Reals group. Whereas kime ($\mathbb{C}$) is an algebraically closed field that naturally extends time. Time is ordered, kime is not! As a complete field, *Kime* represents the smallest natural extension of *Time*.
- **Physics:**
  - The *Problem of Time*: Time has different meanings in quantum mechanics & general relativity; leading to a tension in formulating a Quantum Gravity Theory unifying the two (DOI 10.1007/978-3-319-58848-3).
  - (Base-field) $\mathbb{R}$ and $\mathbb{C}$ based Hilbert-space quantum theories make different predictions (DOI: 10.1038/s41586-021-04160-4).
- *AI/Data Science*: Random IID sampling, Bayesian representations, tensor modeling of $\mathbb{C}$ kimesurfaces & novel analytics.

Wesson (2010); Dinov & Velev (2021); Wang et al. (2022); Zhang et al. (2023); Dinov & Shen (2024).

KPT data model (replicated longitudinal processes)

For time points $t_k \in (0, T]$ and replicates $j = 1, \ldots, N$:

$$\underbrace{\Theta_{j,k}}_{\text{stochastic phase}} \sim \underbrace{\varphi_{t_k}(\theta)}_{\text{latent phase law on } \mathbb{S}^1}$$

$$\underbrace{y_{j,k} \mid \Theta_{j,k}}_{\text{observed measurements}} \sim p\big(y \mid \theta;\, t_k, \mathcal{S}\big)$$

A common likelihood (used in simulations and algorithms):

$$y_{j,k} = \mathcal{S}(t_k, \Theta_{j,k}) + \varepsilon_{j,k}, \qquad \varepsilon_{j,k} \sim \mathsf{N}(0, \sigma^2).$$

Unknown objects:

kime-surface $\mathcal{S}(t, \theta)$ and phase density $\varphi_t(\theta) \in \mathcal{P}$.

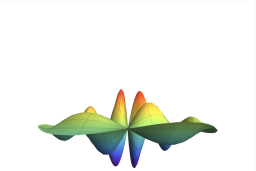

Model Kime-Surface

Problem Solved by Kime-Phase Tomography (KPT)

KPT capability

Given replicated longitudinal observations $\{y_{j,k}\}$, KPT reconstructs a coupled pair

$$(\widehat{\mathcal{S}}(t,\theta),\ \widehat{\varphi}_t(\theta))$$

that explains structured replicate-to-replicate variability as a time-evolving phase distribution on $\mathbb{S}^1$.

- **Interpretability:** $\widehat{\varphi}_t$ quantifies latent state concentration, drift, multimodality.
- **Prediction:** synthetic draws $\theta \sim \widehat{\varphi}_t$ and evaluation of $\widehat{\mathcal{S}}(t,\theta)$ induce predictive distributions.
- **Scalability:** FFT-based spectral updates enable fast inference on dense time grids.

2. Mathematical Foundations

Historical Background: Kaluza-Klein Theory

Theodor Kaluza (1921) developed a *math extension of the classical general relativity theory to 5D*. This included the metric, the field equations, the equations of motion, the stress-energy tensor, and the cylinder condition.

Physicist Oskar Klein (1926) *interpreted Kaluza's 3D+2D theory in quantum mechanical space* and proposed that the fifth dimension was curled up and microscopic.

The topology of the 5D Kaluza-Klein spacetime is $\mathbb{K}_2 \simeq \mathbb{M} \times \mathbb{S}^1$, where $\mathbb{M}$ is a 4D Minkowski spacetime and $\mathbb{S}^1$ is a circle (non-traversable).

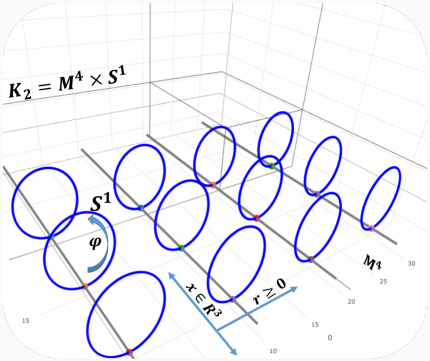

(Kaluza) DOI: 10.1142/S0218271818700017; (Klein) DOI: 10.1007/BF01397481; (Bailin & Love) DOI 10.1088/0034-4885/50/9/001

Ultrahyperbolic PDEs: Wave Equation – Cauchy Initial Data

For ultrahyperbolic PDEs, the (*unconstrained*) initial value problem, determining the solution(s) for a given initial condition, is *ill-posed*. No guarantee of a global well-defined, stable, and unique solution! Nonlocal constraints yield the existence, uniqueness & stability of local and global solutions to the *ultrahyperbolic wave equation* under Cauchy initial data.

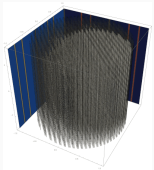

Spacekime Wave Equ Sol

$$\underbrace{\sum_{i=1}^{d_s} \partial^2_{x_i} u := \Delta_x u(x,\kappa)}_{\textit{spacial Laplacian}} = \underbrace{\Delta_\kappa u(x,\kappa)}_{\textit{temporal Laplacian}} =: \underbrace{\sum_{i=1}^{d_t} \partial^2_{\kappa_i} u,}_{} \quad \underbrace{\begin{vmatrix} u_o & = u(x \in D_s;\ (0,\kappa_{-1}) \in D_t) \\ u_1 & = \partial_{\kappa_1} u(x,(0,\kappa_{-1})) \end{vmatrix}}_{\textit{initial conditions (Cauchy data)}}$$

$\exists$ stable local solution over a Fourier frequency region, nonlocal constraints, $|\xi| \geq |\eta_{-1}|$.

$$\hat{u}(\xi,\kappa_1,\eta_{-1}) = \cos(2\pi\kappa_1\sqrt{|\xi|^2-|\eta_{-1}|^2})\hat{u}_o(\xi,\eta_{-1}) + \sin(2\pi\kappa_1\sqrt{|\xi|^2-|\eta_{-1}|^2})\frac{\hat{u}_1(\xi,\eta_{-1})}{2\pi\sqrt{|\xi|^2-|\eta_{-1}|^2}}.$$

Craig & Weinstein (2008); Wang et al. (2022); Dinov & Velev (2021).

Random Sampling from a Probability Law

The SOCR CLT app provides a live demo of drawing from a specific univariate probability distribution, https://socr-clt-webapp.statisticalcomputing.org/.

Sample observability can be used to infer the distribution *likelihood*, but never to predict exact instantaneous outcomes.

Similarly, the phase-law represents the intrinsic variability in repeated longitudinal measurements.

https://socr.umich.edu/TCIU/HTMLs/Chapter6_Kime_Phases_Circular.html.

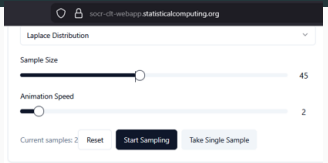

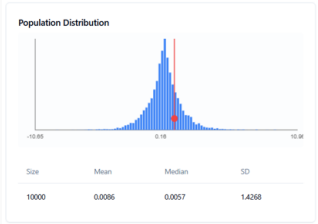

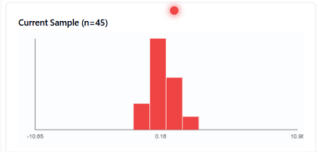

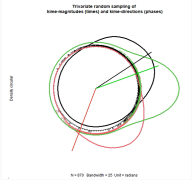

Gauge (rotation) ambiguity and anchoring

A joint circular shift $\theta \mapsto \theta + \alpha(t)$ induces

$$\varphi_t(\theta) \mapsto \varphi_t(\theta - \alpha(t)), \qquad \mathcal{S}(t, \theta) \mapsto \mathcal{S}(t, \theta - \alpha(t)),$$

leaving the composed signal distribution invariant.

- **Rotation-invariant functionals:** $|\widehat{\varphi}_t(n)|$, Sobolev energies, distances.
- **Directional functionals:** mean direction, V-tests, phase-aligned comparisons require anchoring.
- **Anchoring rule (example):** choose $n_\star \geq 1$ with $|\widehat{\varphi}_t(n_\star)| > 0$ and rotate so $\widehat{\varphi}_t(n_\star)$ is real and > 0.

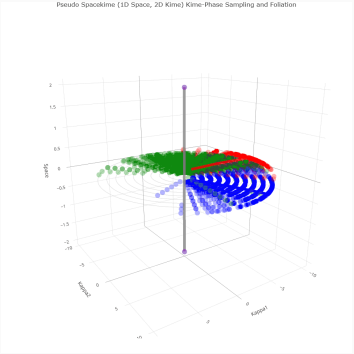

Three Longitudinal Processes over the *Kime manifold*.

3. Inference and Space-Kime Analytics

Space-kime analytics (SKA)

Let observations be indexed by spatial location s (voxel, pixel, sensor, region).

$$y_{j,k}(s) = \mathcal{S}(t_k, \Theta_{j,k}(s); s) + \varepsilon_{j,k}(s), \qquad \Theta_{j,k}(s) \sim \varphi_{t_k}(\cdot; s).$$

- Estimate $\widehat{\varphi}_t(\theta; s)$ and $\widehat{\mathcal{S}}(t, \theta; s)$ across s.
- Spatial regularization on harmonic coefficients (optional).
- Outputs: maps of phase concentration, drift, multimodality; phase-conditioned response maps.

4. Applications and Validation (Simulations)

Validation protocol: two motivating case studies

- **Simulation Study I:** quantum double-slit experiment with run-to-run phase variability.
- **Simulation Study II:** synthetic event-related fMRI ON–OFF design with time-varying latent physiological state.
- Both demonstrate core tenet: *apparent noise* can be decomposed into extrinsic noise + intrinsic kime-phase variability.

Reproducibility

End-to-end computational protocol and figures are provided in the supplemental Rmd notebook / supporting website.

Double-slit: qualitative reconstruction of kime-surface

- Recover $\widehat{\mathcal{S}}(t, \theta)$ from repeated noisy observations.
- Compare true vs. KPT-GEM and KPT-FFT reconstructions.

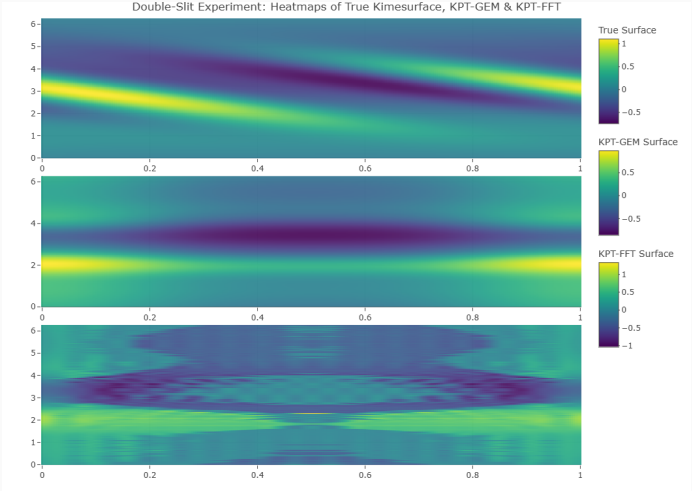

Figure: True vs. KPT reconstructions of $\mathcal{S}(t, \theta)$.

Double-slit: phase recovery metrics across time

- Time-varying KL/JSD/Hellinger/TV between true φ_t and estimated $\widehat{\varphi}_t$.

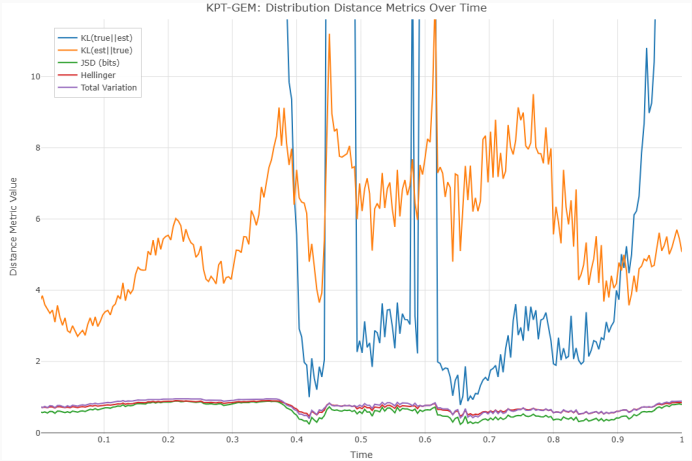

Figure: Phase metrics vs. time (KPT-GEM).

Double-slit: predictive fit and confidence bands

Compare mean MAP curves and confidence bands to observed scatter.

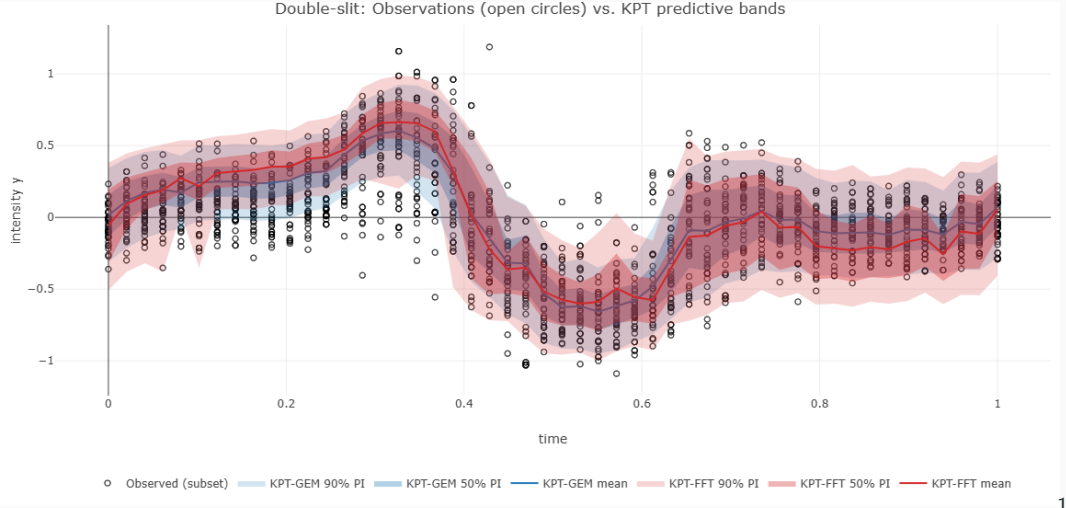

Double-slit: summary metrics

Table: Double-Slit Experiment: Summary metrics comparing true kime-surface vs. KPT reconstructions (KPT-GEM, KPT-FFT).

Algorithm	Mean JSD (bits)	Mean Hellinger	Mean TV	Rel. L2 Surface
KPT-GEM	0.6072	0.7266	0.7532	1.2514
KPT-FFT	0.6101	0.7302	0.7524	1.5167

Double-slit: posterior predictive position density (physics linkage)

- Use recovered kime objects $\{\widehat{\mathcal{S}}(t,\theta), \widehat{\varphi}_t(\theta)\}$ to predict the screen-hit position distribution.
- Two different parameter sets: Observed hits vs. KPT predicted posterior density (two parameter settings).
- Interpretation: KPT transforms run-to-run interference fluctuations into an inferred phase law and a deterministic kime-surface.

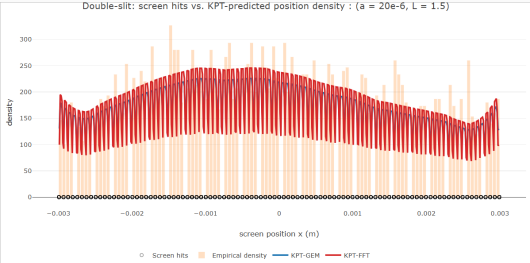

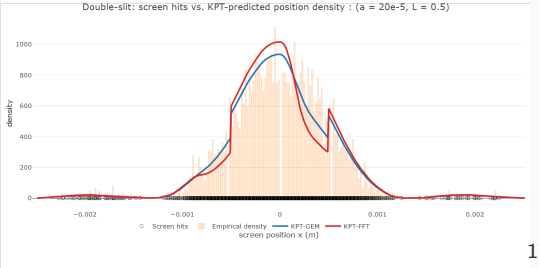

fMRI simulation: setup and motivation

- Simulate event-related ON vs. OFF fMRI design with repeated runs per participant.
- Input to KPT: difference signal $y_{j,r,k} = \mathrm{ON}_{j,r,k} - \mathrm{OFF}_{j,r,k}$ to isolate task activation.
- KPT hypothesis: substantial run-to-run variability arises from intrinsic physiological state, modeled as latent kime-phase $\Theta(t)$.

fMRI: raw simulated trajectories

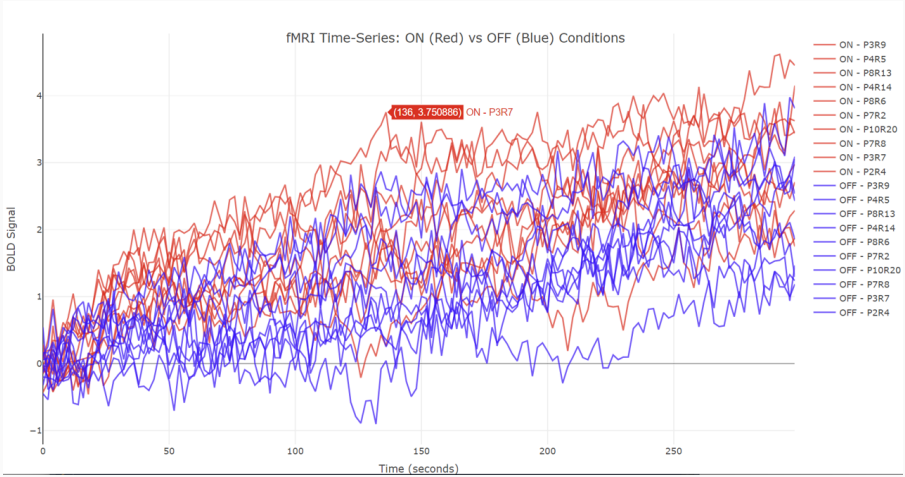

Figure: Examples of simulated ON and OFF fMRI time-courses for random participants (P) and runs (R).

fMRI: phase recovery metrics vs. time (JSD bits)

Symmetric Jensen-Shannon divergence (bits) across time between true & estimated φ_t

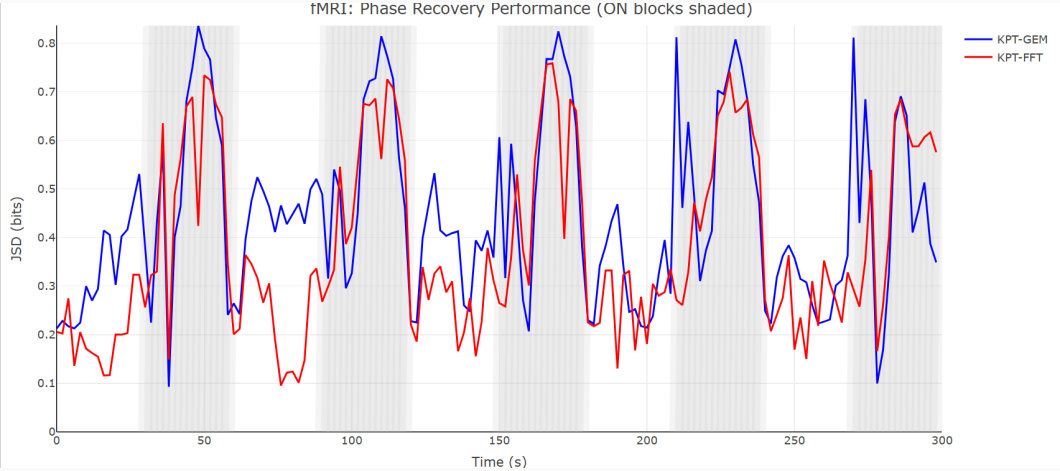

Figure: JSD (bits) across time.

fMRI: example phase at a fixed time slice

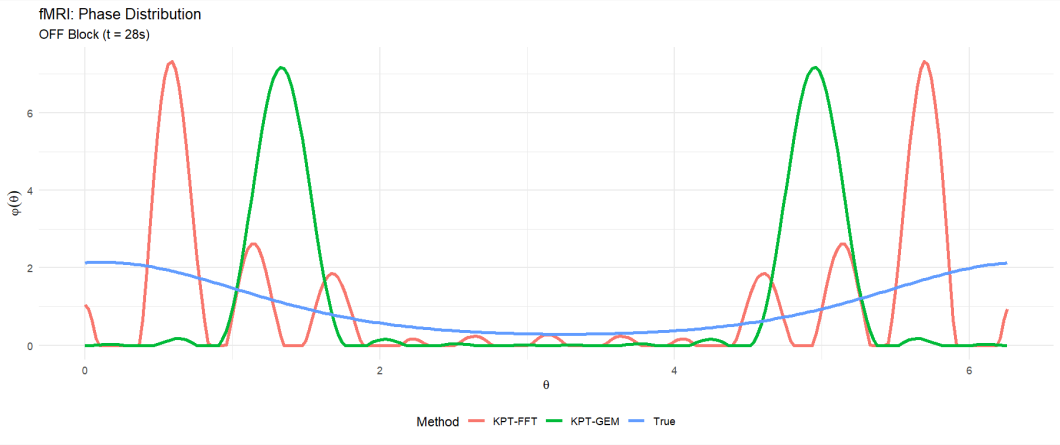

Figure: True phase $\varphi_{t=28s}$ vs. KPT-estimated phases at the same time.

fMRI: kime-surface heatmaps (polar) and 3D reconstructions

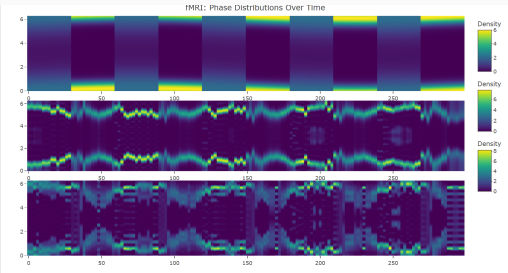

Figure: Polar heatmaps of true vs. KPT kime-surfaces.

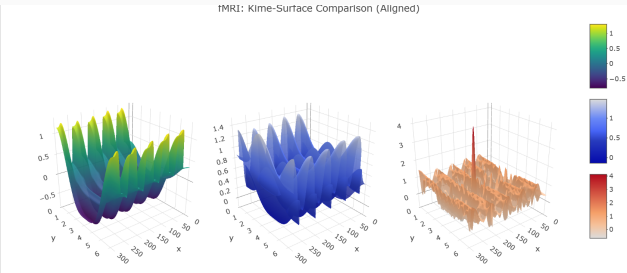

Figure: 3D scenes: True, $\mathcal{S}(t,\theta)$, and Recovered, $\widehat{\mathcal{S}}(t,\theta)$, kimesurfaces.

fMRI Experiment: summary metrics

Table: fMRI Experiment: Summary metrics comparing true kime-surface vs. KPT reconstructions (KPT-GEM, KPT-FFT).

Algorithm	Mean JSD (bits)	Mean Hellinger	Mean TV	Rel. L2 Surface
KPT-GEM	0.4445	0.5942	0.6491	1.5013
KPT-FFT	0.3794	0.5534	0.5588	1.4574

Other Applications

- **Neuroimaging / clinical trials:** run-to-run variability decomposition; QC and stability biomarkers (space-kime maps).
- **Quantum sensing / interferometry:** phase drift tomography and predictive distributions for detection patterns.
- **Coherent imaging / microscopy:** phase-aware stabilization; uncertainty-aware reconstructions.
- **Industrial IoT:** phase-state monitoring for cyclic processes and predictive maintenance.
- **Digital health:** latent physiological state distributions and personalized baselines.

Resources and reproducibility

Websites: https://TCIU.predictive.space/ | https://Spacekime.org/

Rmd-notebook: https://socr.umich.edu/TCIU/HTMLs/TCIU_SK_Appendix03_KPT_DS_fMRI_V5.html

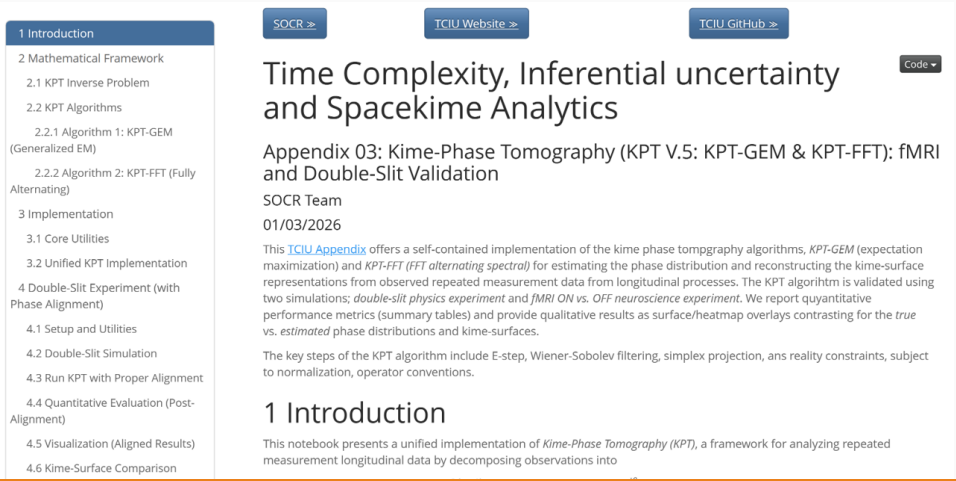

Acknowledgements

- SOCR colleagues, the North Carolina State University, and the University of Michigan.
- Funding: NSF (1916425, 1734853, 1636840) and NIH (R01MH121079, R01MH126137, R41TR004515, T32GM141746, U54DE035412).
- Thank you to many SOCR collaborators, other contributors to the KPT theory, algorithms, and validation protocols, and the broader open-science community.

- Contact: statistics@umich.edu.